8 The $\pi^+ \to e^+\nu_e$ / $\pi^+ \to \mu^+\nu_\mu$ branching ratio

P. Robmann, A. van der Schaaf and P. Truöl

in collaboration with University of Virginia, Charlottesville, USA; Institute for Nuclear Studies, Swierk, Poland; JINR, Dubna, Russia; PSI, Villigen, Switzerland and Rudjer Bošković Intitute, Zagreb, Croatia

(PEN Collaboration)

The theoretical value of the $\pi^+ \to e^+\nu_e$ / $\pi^+ \to \mu^+\nu_\mu$ branching ratio, calculated assuming a universal $Wl_i\nu_i$ coupling strength and the $V - A$ structure of the electroweak interaction, is $1.2353(1) \times 10^{-4}$ [1]. A measurement of the branching ratio would allow sensitive tests of these two fundamental ingredients of the Standard Model. The present experimental result $1.2312(37) \times 10^{-4}$ dates back over thirty years [2] and two new experiments [3] aim at a reduction of the error by almost an order of magnitude.

[1] V. Cirigliano and I. Rosell, JHEP **10** (2007) 5; Phys. Rev. Lett. **99** (2007) 231801.

[2] G. Czapek *et al.*, Phys. Rev. Lett. **70** (1993) 17; D. I. Britton *et al.*, Phys. Rev. Lett. **68** (1992) 3000.

[3] PEN Collaboration, PSI experiment R-05-01 (2005), D. Počanić and A. van der Schaaf, spokespersons; PIENU Collaboration, TRIUMF proposal 1072 (2006), D. Bryman and T. Numao, spokespersons.

8.1 PEN data taking

The PEN experiment took data at PSI during the years 2008 - 2010. The setup varied slightly over the years and the 2010 version is shown in Fig. 8.1. Pions from the πE1 beam line are brought to rest in a plastic scintillator after having crossed a thin scintillator in an intermediate focus 4 m upstream and a degrader scintillator, situated close to the target scintillator. A small time-projection chamber (mini TPC) is used to record the trajectories of the incoming pions.

Decay positrons from $\pi \to e\nu$ and the sequence $\pi \to \mu\nu$, $\mu \to e\nu\bar{\nu}$, are tracked in two cylindrical MWPCs. The positron energy is determined with the help of a spherical 3π Sr pure-CsI calorimeter. A cylindrical plastic scintillator hodoscope in front of the calorimeter is used both for timing and for particle identification (in particular to separate decay positrons and protons from pion reactions) through $\Delta E - E$.

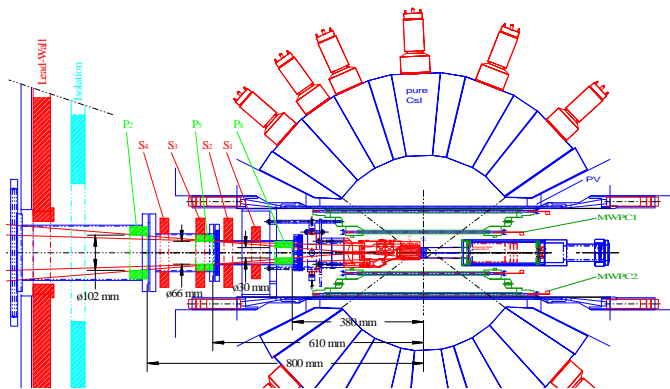Figure 8.2 illustrates how beam pions can be identified by their characteristic velocity and energy loss.

FIG. 8.1 – Cross sections through the PEN setup.
On the right: the target region showing (1) degrader and (3) target scintillators, (2) mini TPC and (4) inner MWPC.
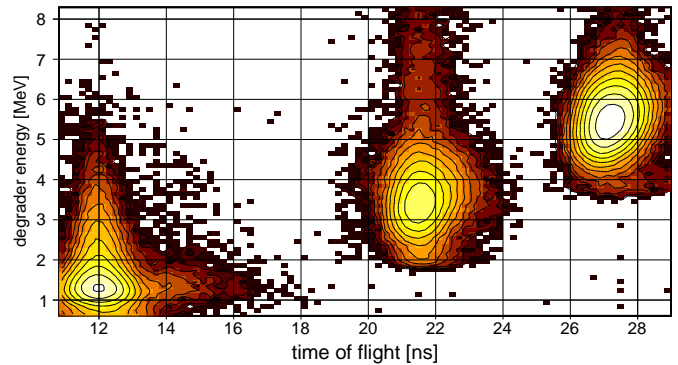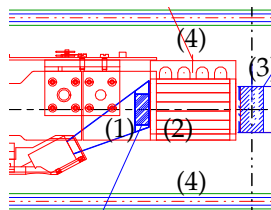

FIG. 8.2 – Degrader energy versus time of flight between an upstream beam counter and the degrader. Events were selected in which a second beam particle is observed, next to the pion required in the readout trigger. The event concentrations, corresponding to (from the left) positrons, muons and pions, reflect the πE1 beam contaminations around 75 MeV/c.
Time of flight is used for an accurate absolute pion energy determination, event by event.
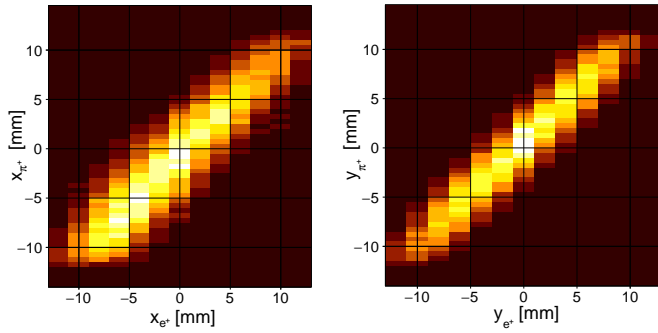
FIG. 8.3 – Correlation between the position coordinates of π^+ and e^+ for e^+ moving vertically (left) and horizontally (right). The correlation, broadened by detector resolutions and by the travel of the intermediate muon, allows for an accurate calibration of the mTPC (x_{π^+} and y_{π^+} are based on charge-division and drift time, respectively).
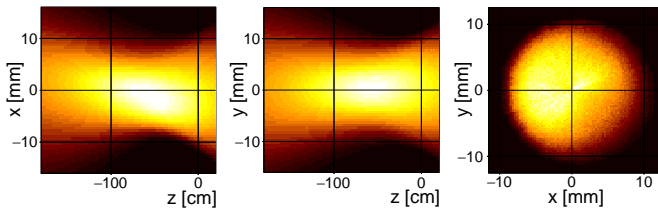

FIG. 8.4 – Pion trajectories as reconstructed with the mini TPC. For these 2009 data the observed target spot is limited radially by a circular $\varnothing = 20$ mm lead collimator situated a few cm upstream of the target. The distribution is off-center in x giving best suppression of the higher-momentum beam positrons situated further to the left.

8.2 The mini TPC beam tracker

Pion trajectories were recorded with the small 4-wire time-projection chamber (TPC) shown in Fig. 8.1. The drift field is in y direction so the y coordinate is determined by drift time. The x coordinate is deduced by charge-division (ratio of signals on both ends of the resistive anode wires). Calibrations were done with selected e^+ MWPC trajectories, as illustrated in Fig. 8.3.

The pion stop location (see Fig. 8.4) is needed (i), to check whether the pion stopped sufficiently far from the target surface to make sure that a decay muon would stay inside the target and (ii), to determine the e^+ path length inside the target.

8.3 The Zurich cylindrical hodoscope

Our workshop contributed all plastic scintillators, in particular the 20-element cylindrical hodoscope. A study was made of its performance by determining the response to protons which give a well-defined dE/dx signal. As can be seen from Fig. 8.5 the position dependence of the light yield differs significantly from the expected smooth exponential distribution and each module has its own "fingerprint", a performance that did not vary over the

years. These maps are used numerically in the data analysis and also taken into account in the detector simulation.

8.4 Target waveform analysis

The classical observables discriminating between the two decay branches are the positron energy and the delay between pion stop and positron emission. The major systematic uncertainty is associated with the few percent of $\pi \to e\nu$ decays depositing less than 52 MeV in the calorimeter where the $\mu \to e\nu\bar{\nu}$ decay dominates by far.

The target waveform analysis aims at testing the occurrence of an intermediate 4.1 MeV muon. The strategy is to remove the signals predicted for pion and positron. The pion time is predicted primarily from the degrader waveform and the pion energy from time-of-flight and degrader energy loss. The positron time is predicted primarily from the plastic hodoscope TDC's and the positron energy from the target trajectory.
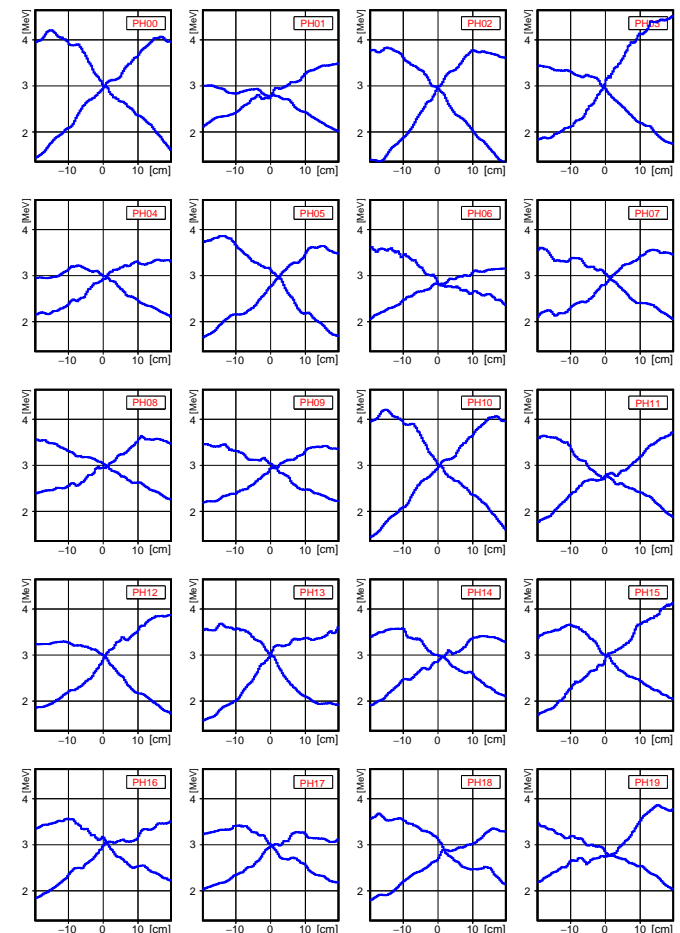

FIG. 8.5 – Position dependence of the light yield observed at the ends of each of the twenty hodoscope staves. Events were selected with 100 MeV protons from pion reactions in the target. Note the irregular behavior varying considerably between the modules.
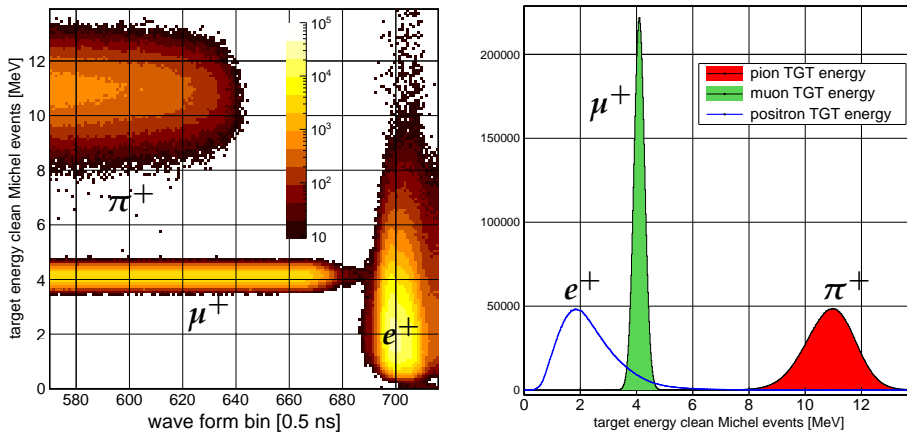
FIG. 8.6 – Results of the target waveform analysis for $\pi \to \mu \to e$ decay chains in which the three target signals are well-separated.

Positrons, which timed the trigger through their signals in the plastic hodoscope, are situated around waveform bin 700. Their parents, the muons, are situated to their left and mono-energetic with $T = 4.1$ MeV since they originate in the decay of a pion at rest. The pions, preceding the muons, deposit typically 11 MeV.

The scheme is optimized by studying events nicknamed "gold-plated Michel events" i.e., events in which the muon signal is well separated from both the parent pion and the daughter positron so all energies can be determined. Figure 8.6 shows for such events the energies and peak positions in the target waveform. Energies have been corrected here for the detector quenching (signal loss for high ionization densities) taken directly from simulation.

Figure 8.7 shows for such events the perfect linear correlations between predicted and observed π^+ and e^+ energies. The left panel of Fig. 8.8 shows how well the pion signal is predicted in time as well. It is very reassuring that all these results depend on nothing but the muon energy calibration. Finally, the right panel of Fig. 8.8 shows how the scheme works when signals do overlap.

8.5   Outlook

PEN finished data-taking five years ago and has been studying these data in great detail ever since. Energy, time and geometry calibrations are done and most features observed are understood and reproduced by simulation.

The question remains when we might expect to "open the box" and finish the project by publishing the branching ratio. Unfortunately, we can't answer that question yet but do hope it happens within the next 1-2 years. Pushing systematic errors far below 0.1% is not easy but really time-consuming is convincing ourselves and the scientific world that we reached that point, in particular if the result should turn out to be unexpected...
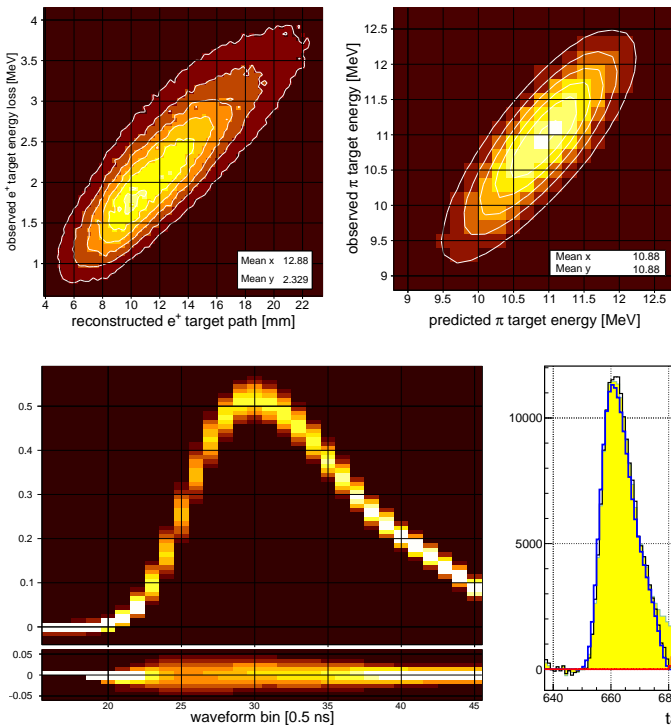
33

FIG. 8.7 – Left: e^+ target energy versus path length. Observed mean dE/dx is 1.81 MeV/cm, or 1.73 MeV/g.
Right: π^+ target energy versus the predicted value based on time of flight and observed degrader energy.
In both cases no adjustments were made other than the energy calibration from the 4.1 MeV muon peak.

FIG. 8.8 – Left: pion waveforms before (upper panel) and after (lower panel) subtraction of the predicted signal. These are thousands of waveforms plotted on top of eachother.
Right: example of the waveform analysis of an event in which the muon lived only 3.5 ns.